Numerical simulation of the signal formation in a scanning electron microscope with remote electrodes

2002 J. Phys.: Condens. Matter 14 13147

(http://iopscience.iop.org/0953-8984/14/48/362)

INSTITUTE OF PHYSICS PUBLISHING JOURNAL OF PHYSICS: CONDENSED MATTER

J. Phys.: Condens. Matter **14** (2002) 13147–13152 PII: S0953-8984(02)54033-9

Numerical simulation of the signal formation in a scanning electron microscope with remote electrodes

V V Sirotkin, E B Yakimov and S I Zaitsev

Institute of Microelectronics Technology, Russian Academy of Sciences, 142432 Chernogolovka, Moscow district, Russia

Received 27 September 2002
Published 22 November 2002
Online at stacks.iop.org/JPhysCM/14/13147

Abstract

In the present paper we simulate and investigate potentiometric current in real three-dimensional geometry. Basic equations are formulated and a numerical method for simulation is developed. We consider a grain boundary, a volume non-homogeneity and near-surface planar defects. Using the latter two defects as examples, it is demonstrated that multi-electrode schemes and a modulation technique offer advantages over the 'classical' two-electrode method of potentiometric division.

1. Introduction

The scanning electron microscope (SEM) in the remote-electrode configuration (REBIC) is extensively used for investigation of high-resistivity and semi-insulating materials (see for example [1]).

The aim of this paper is to select appropriate schemes of the REBIC method for the characterization of three types of defect: high-resistivity grain boundaries, local spatial non-homogeneity of the resistivity and near-surface planar defects. We will consider the 'classical' two-electrode method as well as multi-electrode schemes and a modulation technique (measurements of the first derivative of the collected current, depending on the electron beam inlet position). For the examination of these experimental schemes, we carry out numerical simulation of REBIC signals.

2. Signal formation model and numerical algorithm

A block diagram of the experimental configuration of the REBIC system is shown in figure 1. A focused electron beam falls on a specimen at point P_0. The absorbed current j_0 is divided between several contacts: $j_0 = \sum_{n=1}^{N} j_n$. The current values j_n, $1 \leqslant n \leqslant N$, depend on the specimen shape, the spatial distribution of the specimen conductivity $\sigma(P)$, the positions of the contacts and the beam inlet point P_0. Hence the variation of the inlet point position shows

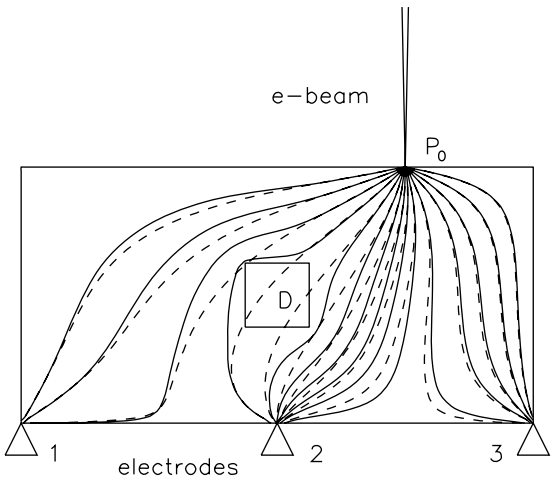

Figure 1. A simplified view of an experiment with a non-uniform distribution of the conductivity inside a specimen (2D cross-section). By measuring currents through contacts 1, 2 and 3 for different positions of the e-beam inlet, it is possible to 'feel' a local non-homogeneity (D). The solid curves are streamlines in the presence of the defect whereas the dashed lines are the result of the calculation for the ideal case without any defect.

promise for use in localization and characterization of spatial non-homogeneities inside the specimen.

The current through the nth contact can be calculated as follows:

$$j_n = \int_{\gamma_n} \sigma(P)\,\vec{\nabla}\phi(P)\cdot \mathrm{d}\vec{s}. \tag{1}$$

The electrostatic potential $\phi(P)$ satisfies the following equation:

$$\vec{\nabla}\cdot[\sigma(P)\,\vec{\nabla}\phi(P)] = -j_0\delta(P, P_0), \qquad P = (x, y, z) \in \Omega, \tag{2}$$

with the boundary conditions

$$\begin{aligned} &\vec{\nabla}\phi(P)\cdot\vec{\nu} = 0, \qquad P \in \partial\Omega\Big\backslash\bigcup_{n=1}^{N}\gamma_n, \\ &\phi(P) = 0, \qquad \text{on contacts } \gamma_n,\ 1 \leqslant n \leqslant N, \end{aligned} \tag{3}$$

where $\vec{\nu}$ denotes the outward unit normal vector.

We emphasize that in the above model, equations (2), and (3) need to be solved separately for each inlet point position. As an alternative approach, we can introduce for each contact the charge collection probability $\psi_n(P)$ [2].

The functions $\psi_n(P)$, $1 \leqslant n \leqslant N$, are the solutions of the following:

$$\vec{\nabla}\cdot[\sigma(P)\,\vec{\nabla}\psi_n(P)] = 0, \qquad P \in \Omega, \tag{4}$$

$$\begin{aligned} &\vec{\nabla}\psi_n(P)\cdot\vec{\nu} = 0, \qquad P \in \partial\Omega\Big\backslash\bigcup_{n=1}^{N}\gamma_n, \\ &\psi_n(P) = 0, \qquad P \in \bigcup_{n\neq m}\gamma_m, \\ &\psi_n(P) = 1, \qquad P \in \gamma_n. \end{aligned} \tag{5}$$

In this case, the current through the nth contact is determined as follows:

$$j_n(P_0) = j_0\psi_n(P_0). \tag{6}$$

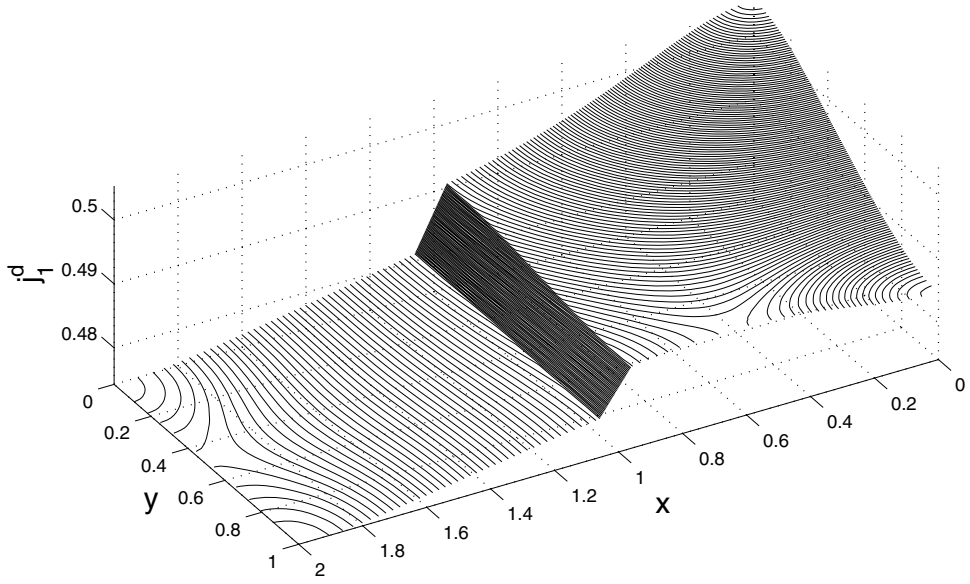

Figure 2. The distribution of the current through one of four contacts in the four-electrode scheme (the contacts are placed at corners on the back of the specimen) for a straight grain boundary with $h^d = 0.1$ and $\sigma^d = 0.1$.

For numerical solution of problems (4) and (5), we use a combination of a finite-difference discretization on adapted non-uniform grids and iterative algorithms for the domain decomposition technique [3].

3. Results of simulation

The following values of the experimental parameters were used for the numerical simulation: the specimen dimensions $L_x = 2$, $L_y = 1$ and $L_z = 1$; the 'ideal' volume conductivity $\sigma^v = 1$; the absorbed current $j_0 = 1$.

Figures 2 and 3 show results for a straight grain boundary, which is described as a thin layer with a value of the conductivity σ^d lower than that of the bulk. The layer is placed in the centre of the specimen in parallel with the yz-plane. The width of the layer is h^d. Figure 2 shows, as an example, the REBIC signal calculated for the experimental scheme involving four contacts localized at the corners on the back of the specimen. One can see that the high resistivity of the grain boundary layer leads to a current drop D. In figure 3 REBIC signals for the two-electrode scheme are presented. From figure 3(b) it follows that the current drop satisfies the equation $D = j_0 R^d/(R^d + R^*)$, where $R^d = \text{constant}(h^d/\sigma^d)$ and R^* is a 'characteristic' resistivity of the specimen.

Note that in the above-mentioned scheme two strip-like contacts coincide with edges, which are parallel to the y-axis and placed on the back of the specimen. Similar strip-like contacts are used in all numerical experiments described below. Moreover, it should be emphasized that in figures 3, 4 and 6 we present REBIC signals calculated as follows:

$$J_n(x_0, L_z) = \frac{1}{L_y} \int_0^{L_y} j_n(x_0, y, L_z)\, \mathrm{d}y.$$

The second set of calculations is performed for a defect of relatively large volume situated in the centre of the specimen ($\sigma^d = 10^{-3}$, $h_x^d = 0.25$, $h_y^d = 0.25$ and $h_z^d = 1$) parallel with

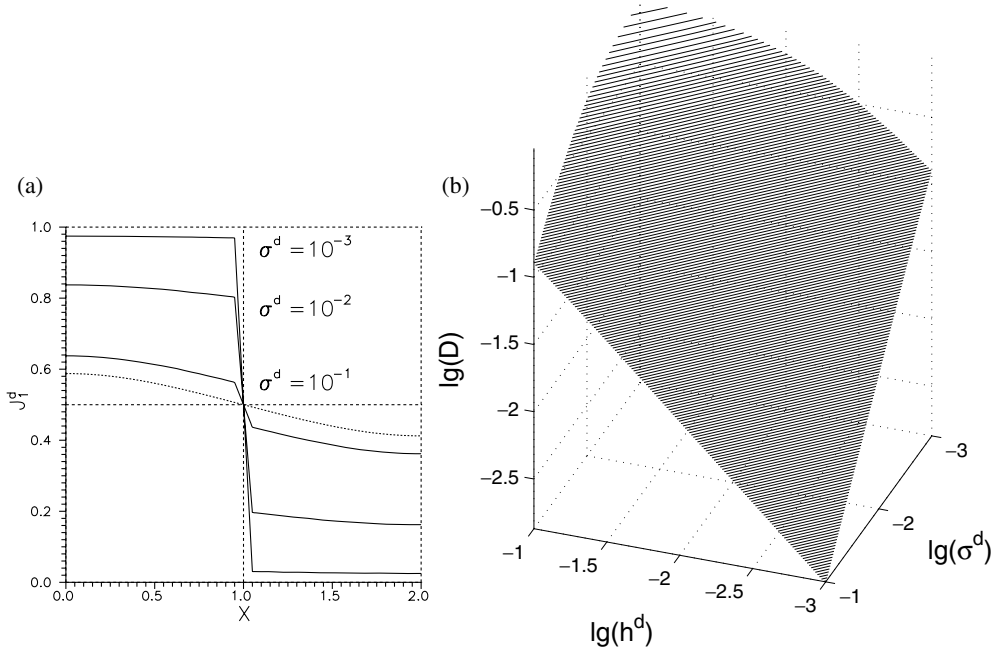

Figure 3. (a) The dependence of the current J_1^d through contact 1 on the x-position of the electron beam for a specimen with a grain boundary at different values of the defect conductivity σ^d and at the defect width $h^d = 0.1$ (solid curves). The dashed curve corresponds to the specimen without any defect. (b) The current drop D as a function of h^d and σ^d.

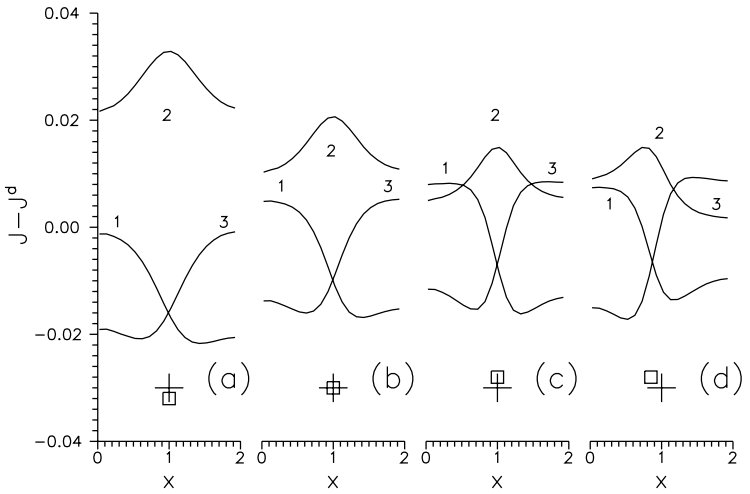

Figure 4. The current differences correspond to contacts 1, 2 and 3 in figure 1 ($J_1 - J_1^d$ for contact 1 and similar values for contacts 2 and 3). The current differences depend on the e-beam position and the position of the volume defect. Panel (b) corresponds to the central position of the defect.

the y-axis. It is found that for better characterization one should use three or more electrodes (figure 1). Figures 4(a)–(d) show current differences $J - J^d$ as a function of the e-beam position and the position of the defect ($J_1 - J_1^d$ for contact 1 and similar values for contacts 2

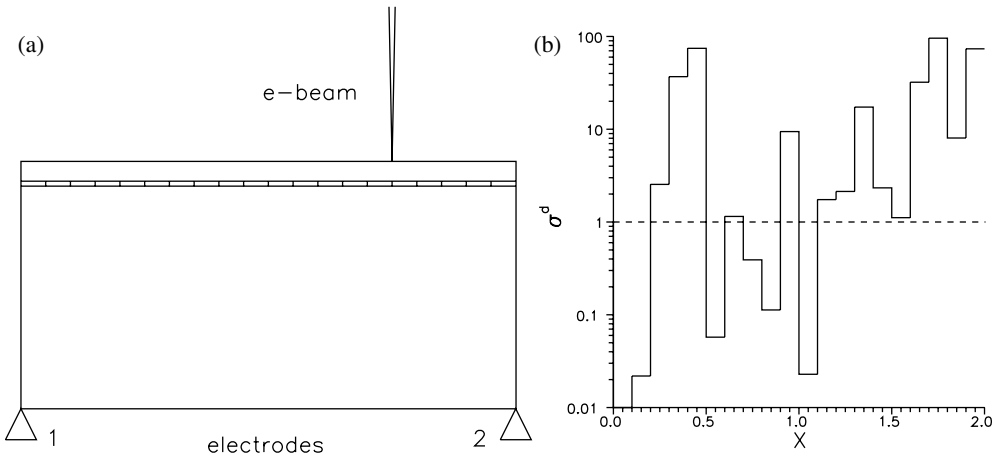

Figure 5. (a) The experimental scheme for the near-surface defect. (b) The distribution of the conductivity in the near-surface defect.

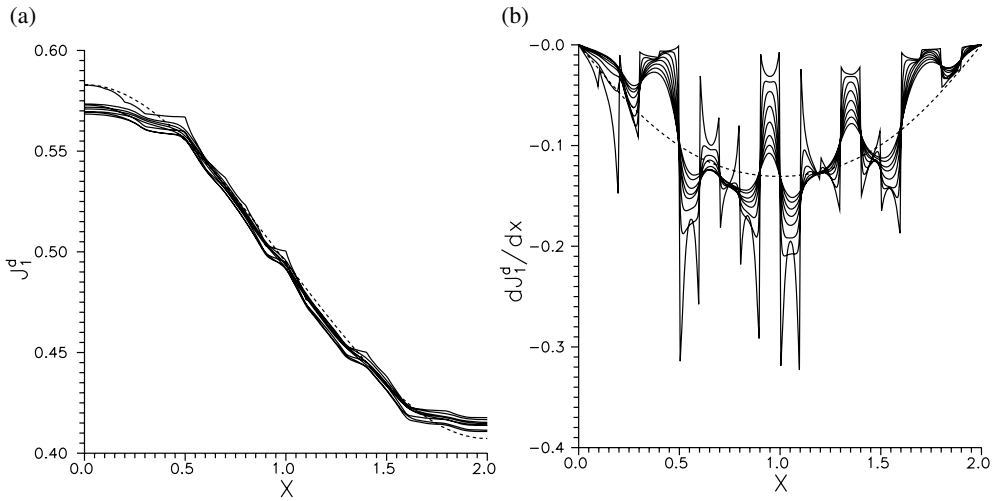

Figure 6. (a) The currents through contact 1 without the near-surface defect (dashed curve) and with the defect (solid curves) situated at different depths y^d. y^d is varied from 0 to 0.07 in steps of 0.01. (b) The derivatives of the currents from figure 6(a).

and 3). Here J_1 is a reference current for contact 1 without any defect, whereas J_1^d is a current in the presence of the defect. From the figures we notice that the intersection of the current differences for contacts 1 and 3 'feels' the lateral position of the defect, whereas to 'feel' a vertical shift of the defect the (central) contact, contact 2, has to be used.

Finally we consider a near-surface defect which consists of a thin layer ($h_x^d = 2, h_y^d = 0.02$ and $h_z^d = 1$) divided into 20 segments to which random values of the conductivity σ^d are assigned in the range 0.01–100 (see figure 5). Figure 6(a) shows the current of contact 1 for the specimen without any defect and for the cases where the defect layer is situated at different depths y^d. It is seen that a high accuracy is needed for the characterization of these defects. We show in figure 6(b) the results of a method in which differential measurements are carried

out by forcing the electron beam to oscillate with a frequency ω during the scanning in the x-direction and only the variable part of the signal corresponding to frequency ω is measured. It is apparent from figure 6(b) that differential measurements give much more information than the direct ones. We emphasize that the central part the curve is very similar to the conductivity profile (figure 5(b)). Simultaneously, figure 6(b) demonstrates that the signal contrast reduces when the depth y^d increases.

4. Conclusions

A mathematical model of signal formation in SEM measurements with remote electrodes has been developed for the case of three defect types: a grain boundary, a local volume defect and a near-surface planar defect. It has been shown that a current jump (drop) may be used for the quantitative characterization of the grain boundaries (and planar defects in general). Two schemes of measurement have been examined numerically: the multi-electrode scheme and the modulation method in which spatial derivatives are measured. It has been found that these methods have better sensitivity and spatial resolution than the 'classical' two-electrode method of potentiometric division.

Acknowledgment

The work of the first author was partially supported by the Russian Foundation of Basic Research (Grants 00-01-00656 and 01-01-97005).

References

[1] Holt D B 2000 *Scanning* **21** 28
[2] Donolato C 1989 *J. Appl. Phys.* **66** 4524
[3] Sirotkin V 2000 *Comput. Math. Appl.* **40** 645